

## Chalcogen Substitution in the Ta<sub>4</sub>P<sub>4</sub>S<sub>29</sub> Tunnel Structure: Synthesis and Structure of TaPS<sub>6</sub>Se

M. EVAIN, M. QUEIGNEC, AND R. BREC\*

*Laboratoire de Chimie des Solides, US 279, Université de Nantes,  
2, rue de la Houssinière, 44072 Nantes Cedex, France*

AND C. SOURISSEAU

*Laboratoire de Spectroscopie I.R., UA 124, Université de Bordeaux I  
351 cours de la Liberation, 33405, Talence, France*

Received November 20, 1986; in revised form April 13, 1987

A compound with a composition close to TaPS<sub>6</sub>Se was prepared either from the elements or from TaPS<sub>6</sub> and Se heated respectively at 630 and 460°C in evacuated silica tubes for 20 days. The crystal symmetry is monoclinic, space group *P2*, with the following cell parameters:  $a = 15.657(2)$  Å,  $b = 6.8714(8)$  Å,  $c = 22.273(3)$  Å,  $\beta = 135.09(1)^\circ$ ,  $V = 1691.7(5)$  Å<sup>3</sup>, and  $Z = 8$ . The structure determination made from 3238 reflections and 244 parameters yielded a reliability factor of  $R = 0.050$ . TaPS<sub>6</sub>Se atomic arrangement is very similar to that of Ta<sub>4</sub>P<sub>4</sub>S<sub>29</sub>, with the same basic tunnel framework in which, instead of ordered sulfur helices, selenium chains, partially substituted by sulfur, are inserted. The chains of composition (Se<sub>8</sub>S<sub>2</sub>) present a periodicity of  $2b$ , but owing to the existence of four different statistically distributed chains, no superstructure is observed. The origin of the network and chain commensurability is related to the chain composition and Se-Se-S angle distortion, along with some small substitution by selenium within the TaPS<sub>6</sub> framework itself. This substitution induces some distortion in the [Ta<sub>2</sub>S<sub>12</sub>] bicapped bipyramids and in the [PS<sub>4</sub>] tetrahedra that constitute the basic structure of the compound. Some elongated interatomic distances were found in the substituted S<sub>2</sub> pairs (mean  $d_{S-S} = 2.123$  Å) and in the mean Ta-Ta distances (mean  $d_{Ta-Ta} = 3.426$  Å). TaPS<sub>6</sub>Se is semiconducting and diamagnetic in agreement with  $d^0$  tantalum cations. © 1988 Academic Press, Inc.

### 1. Introduction

The large number of phases encountered in the *M*-P-S families (*M* being, for example, a transition metal) originates in the numerous oxidation states that can be taken not only by the transition metal, but also by phosphorus and sulfur. Among the *M*-P-S phases where *M* is a Group VA element, the tantalum derivatives (3D)TaPS<sub>6</sub> and (3D)Ta<sub>4</sub>P<sub>4</sub>S<sub>29</sub> were recently obtained (1, 2).

The later phase presents a new combination of a tridimensional network (Ta<sub>4</sub>P<sub>4</sub>S<sub>24</sub>) and polymeric sulfur (S<sub>5</sub>) not bonded to each other. The sulfur chain is trapped in a tunnel formed by the Ta<sub>4</sub>P<sub>4</sub>S<sub>29</sub> framework. It was thought possible to substitute the sulfur helix of Ta<sub>4</sub>P<sub>4</sub>S<sub>29</sub> by selenium, which is known to form a polymeric chain in its elemental form (3). Since the sulfur chain develops in the tunnel of Ta<sub>4</sub>P<sub>4</sub>S<sub>29</sub> over two lengths of the subcell, selenium with a larger atomic size could be expected to lead to a noncommensurate phase. The synthe-

\* To whom correspondence should be addressed.

sis and structure determination of a phase closely corresponding to the analytical formula  $\text{TaPS}_6\text{Se}$  is reported in this article.

## 2. Description of $\text{TaPS}_6$ and $\text{Ta}_4\text{P}_4\text{S}_{29}$ Structures

Prior to studying  $\text{TaPS}_6\text{Se}$ , it may be useful to briefly recall some general features of the two phases  $\text{TaPS}_6$  and  $\text{Ta}_4\text{P}_4\text{S}_{29}$ , since they have many features common to the phase under study. First of all, from an electrochemical point of view, a rather complex charge balance is found for the compounds. For example,  $\text{TaPS}_6$  can be written  $\text{Ta}^{\text{V}}\text{P}^{\text{V}}(\text{S}_2)^{-\text{II}}(\text{S}^{-\text{II}})_4$ .  $\text{Ta}_4\text{P}_4\text{S}_{29}$  may appear to be quite a different compound, but written as  $(\text{TaPS}_6)_4\text{S}_5$  the relationship linking the two compounds is more evident. Thus, the first part of the formula corresponds to what has been called the basic tunnel structure (BTS) and the second one to the sulfur chain trapped in it (2). The charge balance is hence as follows:  $[\text{Ta}^{\text{V}}\text{P}^{\text{V}}$

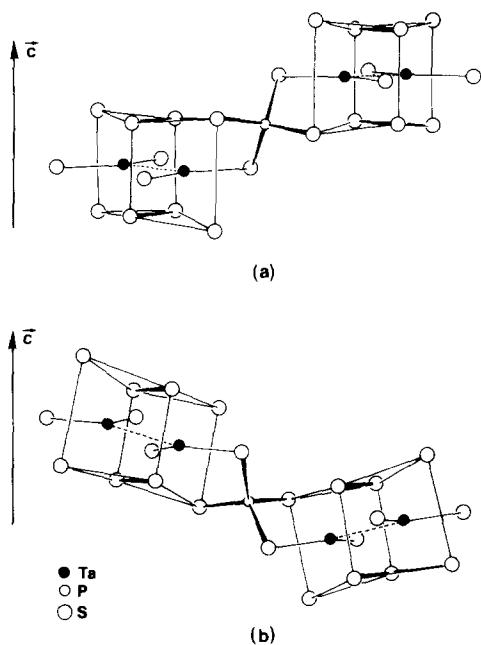


FIG. 1. Arrangement of the biprismatic bicapped  $[\text{Ta}_2\text{S}_{12}]$  units and tetrahedral  $[\text{PS}_4]$  groups in (a)  $\text{TaPS}_6$  and (b)  $\text{Ta}_4\text{P}_4\text{S}_{29}$ .

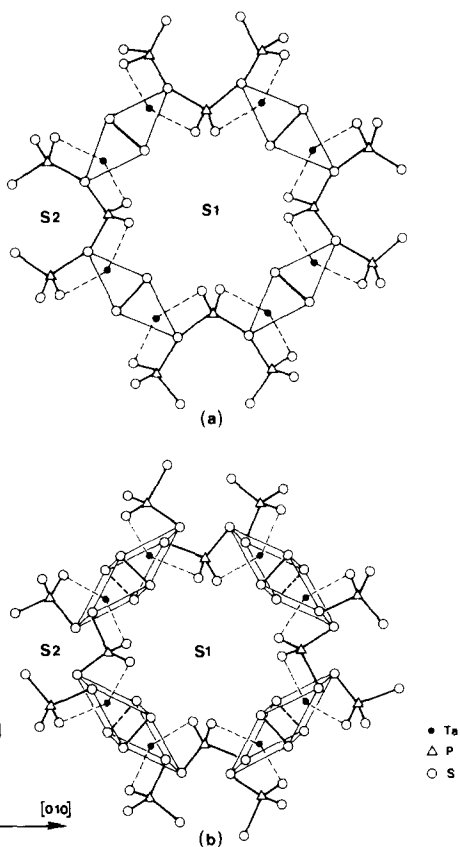


FIG. 2. Partial projection, along their  $c$  axis, of (a)  $\text{TaPS}_6$  and (b)  $\text{Ta}_4\text{P}_4\text{S}_{29}$  structures, showing the large (S1) and narrow (S2) space left by the structural array.

$(\text{S}_2)^{-\text{II}}(\text{S}^{-\text{II}})_4)_4\text{S}_5^0$ . Actually, the main difference between both compounds does not come from their building blocks, which are about the same, but from the way that they span the crystal space as explained below.

Both phases are built from a  $[\text{Ta}_2\text{S}_{12}]$  bicapped trigonal prism and a  $[\text{PS}_4]$  tetrahedron. The two units are alternatively linked to one another as indicated in Fig. 1, the  $[\text{PS}_4]$  tetrahedra being formed from a capping and the edge sulfur from two neighboring prisms. In the interconnected groups, the  $[\text{Ta}_2\text{S}_{12}]$  biprisms that have their edges parallel to the  $c$  axis of the tetragonal cell in  $\text{TaPS}_6$  are tilted relative to that axis in  $\text{Ta}_4\text{P}_4\text{S}_{29}$ . However, for the purpose of the schematic representation of both structures (4),

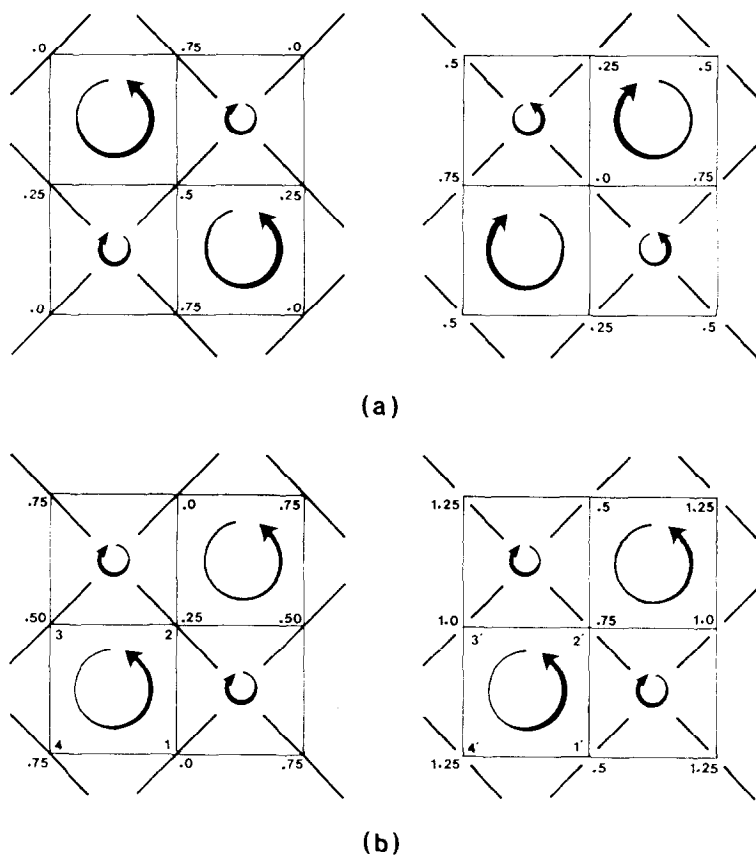


FIG. 3. Schematic representation of the two interlocking systems constituting (a) TaPS<sub>6</sub> and (b) Ta<sub>4</sub>P<sub>4</sub>S<sub>29</sub> structures. Segments represent the [Ta<sub>2</sub>S<sub>12</sub>] biprisms; figures are rounded elevations of the tantalum atoms of these units. Arrows indicate the upward direction of rotation of the [Ta<sub>2</sub>S<sub>12</sub>] groups. Both (a) and (b) correspond to the interlocked chains of the structures.

the difference due to the tilting of the groups can be ignored, as is clearly seen in Fig. 2, where a basic portion of the two structures are represented. From that structure projection, one observes that the structural array leaves large and narrow empty spaces (S1 and S2). In symbolizing the [Ta<sub>2</sub>S<sub>12</sub>] biprisms by a straight line joining the Ta-Ta axis and ignoring the linking (PS<sub>4</sub>) groups, we obtain the representation shown in Fig. 3, corresponding to both TaPS<sub>6</sub> and Ta<sub>4</sub>P<sub>4</sub>S<sub>29</sub>. Arrows indicate the way the biprisms go up the *c* axis.

Actual structure representation is achieved by putting both pictures above each other (Fig. 4). In the case of Ta<sub>4</sub>P<sub>4</sub>S<sub>29</sub>

BTS, the same two arrangements preserve the original large space (S1) that becomes a wide tunnel. On the contrary, in TaPS<sub>6</sub> S1 and S2 areas are above each other and one obtains two interpenetrating (or interlocking) arrangements (which is also the case for Ta<sub>4</sub>P<sub>4</sub>S<sub>29</sub>) but without the large tunnel.

### 3. Experimental

Because Se-Se distances are larger than the S-S ones, a smaller selenium content was expected to substitute for the sulfur chain in Ta<sub>4</sub>P<sub>4</sub>S<sub>29</sub> (TaPS<sub>6</sub>, S<sub>1.25</sub>) and a TaPS<sub>6</sub>/Se ratio of 1/1 was chosen. This molecular ratio proved fairly justified, within er-

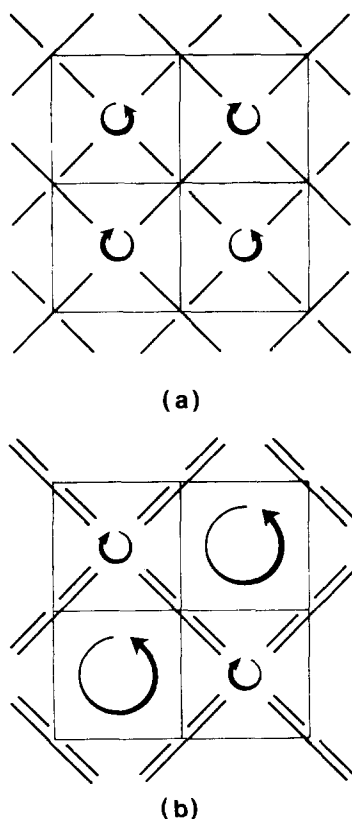


FIG. 4. Final schematic construction of (a)  $\text{TaPS}_6$ , and of (b)  $\text{Ta}_4\text{P}_4\text{S}_{29}$  basic tunnel structure.

ror, by the elemental analysis obtained from the substituted crystals (Table I).

To achieve the chemical synthesis of the phase, two different pathways were used. The first consisted in heating the stoichiometric proportions of the elements in an evacuated silica tube at  $630^\circ\text{C}$  for 20 days, followed by a 10-hr cooling.

Because of the structure similarities between  $\text{TaPS}_6$  and  $\text{Ta}_4\text{P}_4\text{S}_{29}$ , it was believed that little energy would be necessary if  $\text{TaPS}_6$  was allowed to react with 1 mole of selenium. Thus, heating  $\text{TaPS}_6$  and Se in a 1/1 ratio at  $460^\circ\text{C}$  for 3 weeks yielded the same phase as the previous procedure. In both cases, well-shaped and crystallized black needles grew at the sample's surface. Their analysis was conducted with a micro-

probe (microsonde Ouest CNEXO) using  $\text{Ta}_4\text{P}_4\text{S}_{29}$  and  $(\text{TaSe}_4)_2\text{I}$  single crystals as standards. The results (Table I) are in fair agreement with the stoichiometric formula  $\text{TaPS}_6\text{Se}$ , although, indeed, because of the special features of the structure (see structure description), the selenium amount may not be exactly equal to one. For convenience, the stoichiometric formula will be used in the article. Single-crystal X-ray studies showed patterns indistinguishable from that of  $\text{Ta}_4\text{P}_4\text{S}_{29}$ , except for the  $2c$  superstructure due to the sulfur chain (2) which completely vanished. Powder spectra could be indexed with  $\text{Ta}_4\text{P}_4\text{S}_{29}$  tetragonal cell parameters, but least-squares refinement conducted in this symmetry did not yield the best goodness of fit. A monoclinic cell, derived from the tetragonal one according to the relation,

$$\begin{bmatrix} a_m \\ b_m \\ c_m \end{bmatrix} = \begin{bmatrix} 1 & 0 & 0 \\ 0 & 0 & \frac{1}{2} \\ 1 & 1 & 0 \end{bmatrix} \begin{bmatrix} a_t \\ b_t \\ c_t \end{bmatrix},$$

had to be taken instead and  $\text{TaPS}_6\text{Se}$  new monoclinic parameters (Table I) were correctly refined. This was done from the 71 first reflections of a Guinier powder spectrum (Table II) (Guinier Nonius FR552,  $\lambda\text{CuK}\alpha_1 = 1.54056 \text{ \AA}$ , Si as standard). Final refinement yielded a  $\text{TaPS}_6\text{Se}$  cell volume of  $V = 1691.7(5) \text{ \AA}^3$ , quite larger than that of  $\text{Ta}_4\text{P}_4\text{S}_{29}$  subcell with  $V = 1655.0(2) \text{ \AA}^3$ .

A volume increase may appear normal for a substitution of sulfur by selenium. However,  $\text{Ta}_4\text{P}_4\text{S}_{29}$  BTS may be considered as a frame rigid enough to allow rather little expansion, should only the sulfur atom of the tunnel be substituted. This consideration is probably still more true for the parameter along the chain, which nevertheless increased from  $6.8258(4)$  to  $6.8714(8) \text{ \AA}$ . Indeed, this information, indicating possible substitution in the BTS, is valuable and must be considered in the course of the structure refinement study (see below).

TABLE I  
ANALYTICAL AND CRYSTALLOGRAPHIC DATA: PARAMETERS OF THE X-RAY DATA COLLECTION  
AND REFINEMENT

---

Physical, crystallographic, and analytical data

Formula: PTaS<sub>6.15</sub>Se<sub>1.1</sub>. Molecular weight: 495.96 g  
 Calculated weight fraction concentration:  
 P: 6.2%, S: 39.8%, Se: 17.5%, Ta: 36.5%  
 Microprobe analysis:  
 No. 1 = P: 6.2%, S: 39.4%, Se: 15.9%, Ta: 37.9%  
 No. 2 = P: 6.5%, S: 40.5%, Se: 17.3%, Ta: 34.7%  
 Crystal symmetry: Monoclinic. Space group: *P2*  
 Cell parameters (293 K):  
 $a = 15.657(2) \text{ \AA}$ ,  $b = 6.8714(8) \text{ \AA}$ ,  $c = 22.273(3) \text{ \AA}$ ,  $\beta = 135.09(1)^\circ$ ,  $V = 1691.7(5) \text{ \AA}^3$ ,  $Z = 8$   
 Density:  $\rho_{\text{cal}} = 3.813 \text{ g/cm}^3$   
 Absorption factor:  $\mu: \lambda\text{MoK}\alpha: 186.1 \text{ cm}^{-1}$   
 Crystal size:  $0.034 \times 0.075 \times 0.55 \text{ mm}^3$

Data collection

Temperature: 293 K. Radiation: MoK $\alpha$   
 Monochromator: oriented graphite (002). Scan mode:  $\omega/2\theta$   
 Recording angle range:  $4^\circ\text{--}30^\circ$ . Scan angle:  $0.95 + 0.35 \tan \theta$   
 Values determining the scan speed:  
 $\text{SIG}_{\text{pre}}: 0.75$ ,  $\sigma: 0.08$ ,  $\text{NPI}_{\text{pre}}: 10^\circ \text{ min}^{-1}$ ,  $T_{\text{max}} = 90 \text{ sec}$   
 Standard reflections: 522, 712, 604. Periodicity: 3600 sec  
 $\text{ABS}_{\text{max}}: 0.5454$ ,  $\text{ABS}_{\text{min}}: 0.1663$ ,  $\text{ABS}_{\text{ave}}: 0.4644$

Refinement conditions

Reflections for the refinement of the cell dimensions: 25  
 Recorded reflections in the quarter-space: 10,363  
 Utilized reflections: 3238 with  $I \geq 3\sigma(I)$   
 Refined parameters: 244  
 Reliability factors:  $R = \Sigma ||F_o| - |F_c|| / \Sigma |F_o|$   
 $R_w = [\Sigma w(|F_o| - |F_c|)^2 / wF_o^2]^{1/2}$

Refinement results

$R = 0.05$ ,  $R_w = 0.057$   
 Difference Fourier maximum peak intensity:  $3.8(5) \text{ e} / \text{\AA}^3$

---

At first, the condition limiting possible reflections on the (*hkl*) planes appeared to be *h0l* with  $l = 2n$ , indicating *Pc* or *P2/c* as possible space groups. Recording the diffraction pattern of a better crystallized and bigger single crystal indicated however very weak (*h0l*) reflections with  $l = 2n + 1$  (77 of them with  $I \geq 3\sigma(I)$ ) out of 3238 reflections were kept for the refinement calculations). *P2*, *P2/m*, or *Pm* were then considered as possible TaPS<sub>6</sub>Se space groups. Best refinement was obtained with the *P2* group.

The crystal selected for intensity record-

ing on the Nonius CAD4 diffractometer was a small parallelepiped elongated along the monoclinic *b* axis (Table I). From the crystal size and shape, intensities were corrected for absorption, using, as for the data reduction, structure solution, and refinement, the SDP-PLUS program chain (1982 version) of Enraf-Nonius written by Frenz (6) (Table I).

#### 4. Structure Refinement

Since the TaPS<sub>6</sub>Se X-ray powder pattern was very similar to that of Ta<sub>4</sub>P<sub>4</sub>S<sub>29</sub>, it sug-

TABLE II  
TaPs<sub>6</sub>Se X-RAY POWDER DIFFRACTION DATA

$d_{\text{obs}}$ (Å)	$d_{\text{calc}}$ (Å)	$hkl$	$100 \times I/I_0^a$	$d_{\text{obs}}$ (Å)	$d_{\text{calc}}$ (Å)	$hkl$	$100 \times I/I_0^a$
11.06	11.14	10 $\bar{2}$	2	2.3118	2.3118	42 $\bar{1}$	1
	11.05	100		2.2998	2.9997	51 $\bar{1}$	1
7.83	7.86	00 $\bar{2}$	29.7	2.2894	2.2879	52 $\bar{4}$	7.3
	7.83	20 $\bar{2}$		2.2424	2.2428	130	0.4
5.84	5.85	11 $\bar{2}$	100	2.2175	2.2187	52 $\bar{3}$	1.3
	5.83	110		2.2107	2.2108	500	1.4
5.533	5.527	200	7.5	2.1766	2.1770	131	9.8
5.166	5.164	21 $\bar{2}$	0.4		2.1765	23 $\bar{1}$	
4.948	4.959	10 $\bar{2}$	36	2.1131	2.1135	116	8.3
	4.942	30 $\bar{2}$			2.1129	52 $\bar{2}$	
4.905	4.905	111	7.4	2.1042	2.1045	510	2.3
	4.899	21 $\bar{1}$		2.0772	2.0781	626	2
4.313	4.307	210	10.6	2.0657	2.0639	125	0.6
4.157	4.156	31 $\bar{3}$	0.5	2.0568	2.0577	304	2
4.018	4.012	31 $\bar{2}$	0.5		2.0567	719	
3.686	3.685	300	3.8	2.0498	2.0562	215	0.7
3.493	3.494	40 $\bar{2}$	0.2		2.0494	715	
3.436	3.436	020	2.1	2.0254	2.0250	33 $\bar{1}$	0.3
3.321	3.320	41 $\bar{3}$	0.9	2.0062	2.0061	624	0.9
3.283	3.283	12 $\bar{2}$	0.9	1.9891	1.9896	521	0.6
	3.281	120			1.9655	008	
3.246	3.247	310	0.2	1.9654	1.9643	135	4
3.115	3.114	41 $\bar{2}$	5.4		1.9588	1.9571	
3.086	3.088	12 $\bar{3}$	9.4	1.9274	1.9279	62 $\bar{3}$	2
	3.087	22 $\bar{3}$		1.9148	1.9155	43 $\bar{2}$	1.6
	3.085	121		1.8649	1.8651	713	1.3
	3.083	221		1.8400	1.8400	2110	0.9
2.919	2.918	220	0.5	1.8396	136		
2.870	2.873	023	4.7	1.8332	1.8340	216	1.9
	2.870	323			1.8335	8110	
2.846	2.847	311	3	1.8332	1.8327	62 $\bar{2}$	0.5
	2.845	41 $\bar{1}$			1.8317	5012	
2.821	2.824	122	4.7	1.8161	1.8163	70 $\bar{2}$	0.5
	2.821	32 $\bar{2}$		1.7974	1.7979	53 $\bar{3}$	0.9
2.7996	2.8005	514	1.3	1.7555	1.7560	71 $\bar{2}$	1.8
2.7617	2.7634	400	2	1.7175	1.7179	040	0.2
2.6930	2.6922	32 $\bar{1}$	3.7	1.7069	1.7065	411 $\bar{2}$	1.3
2.6727	2.6732	51 $\bar{3}$	2.5		1.7061	028	
2.6077	2.6095	606	4.1	1.6929	1.6930	814	1
2.5786	2.5803	418	9.5	1.6852	1.6847	1110	0.5
2.5643	2.5639	410	9.3	1.6757	1.6765	439	2
2.5453	2.5460	42 $\bar{3}$	1.4		1.6758	539	
2.5128	2.5128	320	9.3	1.6468	1.6756	918	0.3
2.4959	2.4964	51 $\bar{2}$	0.4		1.6468	611	
2.4707	2.4712	604	5.1	1.6453	1.6458	71 $\bar{1}$	0.3
2.4500	2.4497	422	0.6	1.6137	1.6146	721 $\bar{2}$	0.2
2.4074	2.4081	61 $\bar{5}$	0.3		1.6140	311 $\bar{2}$	
2.3255	2.3254	614	1	1.5961	1.5963	138	0.4

<sup>a</sup> Intensities calculated with the LAZY PULVERIX program (5).

gested the same type of atomic arrangement for the BTS of this latter phase, and refinement calculations were hence started using the same structure frame. The calculation converged rapidly, but, owing to strong correlations between atoms related by the pseudo-*c*/2 glide plane, drifting of the atoms thermal factors could not be prevented, and the anisotropic thermal coefficients  $\beta_{ii}$  of the corresponding atoms were set identical and kept as such thereafter.

The refinement showed proper tantalum and sulfur positions and parameters. On the other hand, the phosphorus atoms presented very high thermal factors, away from the range for phosphorus in tetrahedral [PS<sub>4</sub>] groups (7–18). Such phenomenon is often the consequence of partial site filling by an atom. The refinement of the occupancy ratio was introduced in the calculation, with an isotropic thermal factor that reached then expected lower values. Indeed, the amount of phosphorus became too small and other positions had to be found. Extra tetrahedral voids exist in the structure as is seen in Fig. 5. These sites located at about  $z \approx 0.5$  above the first filled ones are empty in Ta<sub>4</sub>P<sub>4</sub>S<sub>29</sub>. Their partial occupancy was revealed by a Fourier difference map and their subsequent introduction in the calculation resulted in the lowering of the reliability factor. The total phosphorus amount became, within error, close to the analytical result, but correlated shifts took place between the occupancy ratio  $\tau$  and the thermal factors. These latter were kept at the value they have in Ta<sub>4</sub>P<sub>4</sub>S<sub>29</sub> ( $B = 0.9 \text{ \AA}^2$ ) and  $\tau$  was refined. It was found that half of the position has a  $\tau \approx 0.6$  and the other half a  $\tau \approx 0.4$ . It was thus chosen to take the values  $\tau \approx 0.6$  and  $0.4$  and to resume the refinement with free B factors (see Table V). Anisotropic refinement could not be done.

It is to be pointed out that the phosphorus positions with  $\tau = 0.4$  correspond to a right-handed rotation of the (Ta<sub>2</sub>S<sub>12</sub>–PS<sub>4</sub>–

Ta<sub>2</sub>S<sub>12</sub>–PS<sub>4</sub> . . .) groups and the one with  $\tau = 0.6$  to a left-handed rotation of the same groups. Also, in Ta<sub>4</sub>P<sub>4</sub>S<sub>29</sub> the sulfur helix was found to rotate like the units of the BTS, and this is an important point to be discussed in the following section.

At that step of the refinement procedure, a calculation of some important interatomic distances, in particular that of the sulfur–sulfur bonds in the (S<sub>2</sub>)<sup>-II</sup> groups indicated, on all the anionic pairs, too large distances between 2.10 and 2.15 Å. Distances in such anions are equal to  $2.05 \pm 0.01 \text{ \AA}$  for all the other *M*–P–S phases (7–18). In addition, the equivalent thermal factors ( $B_{\text{eq}}$ ) of these sulfur atoms gave mean values of  $B_{\text{eq}} \sim 1 \text{ \AA}^2$ , somewhat lower than the average obtained on the other sulfur anions of the structure ( $B_{\text{eq}} \approx 1.4 \text{ \AA}^2$ ). Moreover, the Ta–Ta distances of the tantalum cations situated on each side of (S<sub>2</sub>)<sub>2</sub> rectangle constituted by (S<sub>2</sub>) pairs were quite longer (Ta–Ta = 3.43 Å) than in TaPS<sub>6</sub> (3.37 Å) and Ta<sub>4</sub>P<sub>4</sub>S<sub>29</sub> (3.38 Å).

These data implied some small statistical substitution of sulfur by the selenium atoms at the dianionic sites. This conclusion is to be compared with the observation that the cell parameters (and particularly the *b* axis) had substantially and unexpectedly increased upon selenium substitution. A calculation considering the interatomic distances in S<sub>2</sub><sup>-II</sup> and Se<sub>2</sub><sup>-II</sup> groups and taking into account the atomic numbers gave a  $\approx 5\%$  substitution. This was introduced in the calculation, the atomic coordinates and thermal factors of S and Se of the same sites being refined but kept identical to each other and the substitution ratio being left at its evaluated value.

BTS structure refinement with anisotropic thermal factors (except for phosphorus kept isotropic) led to  $R = 0.077$ . At that point of the calculation, only the selenium atoms in the tunnel had to be located. A study of the data statistics revealed homogeneous reliability factor values for the



various (*hkl*) groups, except for the (*h0l*) and (*h2l*) family with respectively  $R = 0.148$  and  $0.097$  (Table III). A difference Fourier peak search revealed the last positions in the tunnel of the BTS, but with rather weak peaks. A density map was hence drawn around the tunnel axis. It revealed peaks elongated mostly in the *b* direction, consistently with some random distribution of the atoms, and with fuzzy maxima not corresponding to simple classical Se–Se bond lengths nor to S–S distances or even to S–Se ones (if one supposes some sulfur substitution in a selenium chain).

The introduction of these atoms on the more significant positions of the density map produced a significant lowering of the reliability factor, particularly of the (*h0l*) and (*h2l*) groups. In addition, the newly introduced atoms showed, in agreement with the idea of complete disorder, very high thermal motion ( $B_{\text{eq}} \approx 10 \text{ \AA}^2$ ). The refined occupancy ratio gave, within error, a crystal composition in the elemental analysis range. In view of the residual, this first calculation was quite satisfactory with a value of  $R = 0.047$  (and  $R_w = 0.053$ ) and homogeneous data of the different (*hkl*) families as

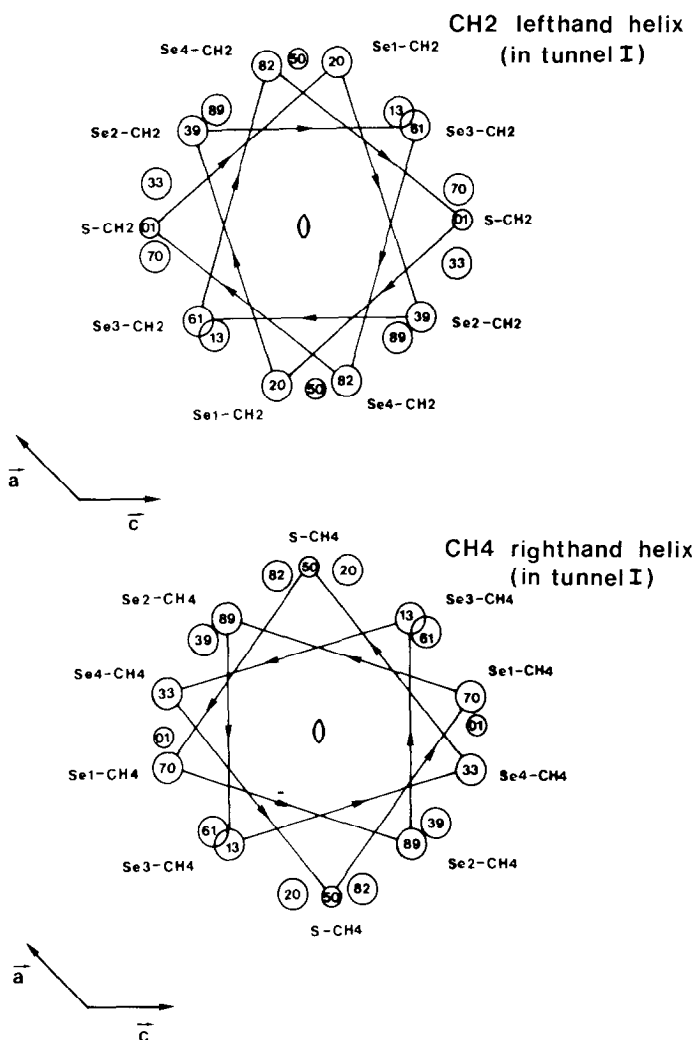
shown by the statistical analysis (Table III). However from a filling of the tunnels standpoint, a true atomic disorder along the tunnels should have given rise to constant electronic density, which was not the case for the PTaPS<sub>6</sub>Se phase, consistent with the fact that the positions introduced were remaining rather stable in their sites during the refinement. One had thus to find a meaning to the many positions found in the tunnel which, at first sight, were senseless. The most plausible hypothesis was that of the occurrence of chains (with identical atomic sequences) having different positions within the tunnels introduced, at the X-ray diffraction level (that yields average structures), a macroscopic disorder.

An exhaustive research of chains of atoms spanning the crystal space in the same way as those present in Ta<sub>4</sub>P<sub>4</sub>S<sub>29</sub> was undertaken. A somewhat complex solution appeared to satisfy both the interatomic distances and the bonds angles. The answer to the problem consisted of splitting the initial positions (corresponding to the electronic map elongated peaks) into two distinct positions within each independent tunnel. This gave four chains: CH1, CH2, CH3, and CH4, only two being independent, i.e.,

TABLE III  
STATISTICAL DATA BASED ON GIVEN VALUES OF *k*, BEFORE AND AFTER SELENIUM INTRODUCTION

Values of <i>k</i>	Number of contributions	Average $F_{\text{obs}}$	Without Se in tunnel		With Se in tunnel	
			<i>R</i>	$R_w$	<i>R</i>	$R_w$
0	397	130	0.148	0.182	0.039	0.040
1	568	112	0.066	0.072	0.043	0.049
2	559	115	0.097	0.133	0.046	0.055
3	481	109	0.062	0.074	0.047	0.058
4	347	114	0.064	0.078	0.048	0.058
5	296	113	0.053	0.061	0.048	0.057
6	275	106	0.066	0.079	0.052	0.065
7	211	96	0.057	0.066	0.052	0.060
8	105	102	0.064	0.074	0.056	0.066
9	24	130	0.075	0.085	0.063	0.075



FIG. 7. Same as Fig. 6 for chains CH<sub>2</sub> and CH<sub>4</sub> in tunnel I.

finement was resumed with the four chains, the  $x$ ,  $y$ , and  $z$  coordinates being kept at the values obtained through the separate refinements (and with  $\tau = 0.25$ ), only the temperature factor being varied, except with the following constraints. Let us recall that, because of the pseudo-symmetry  $P2/c$ , the atoms corresponding to each other through the  $c$  glide plane had their  $B$  factors set equivalent. The same constraint on the selenium  $B$  factors had to be added between

atoms originating from the above position splitting. They were too close to avoid correlated shifts.

The refinement carried out with an occupancy ratio of  $\tau = 0.25$  for all atoms and assuming only selenium atomic positions showed that four atoms had very high thermal factors.

Also, the distances between these atoms and their closest neighbor in the chains averaged 2.2 Å, smaller than the Se-Se mean

distance of 2.3 Å, indicative of sulfur substitution to give a (Se<sub>4</sub>-S-Se<sub>4</sub>-S) chain. Introduction of sulfur on these positions led to acceptable *B* parameter values.

For reasons explained below, the occupancy ratio of the chains atomic positions

were not kept at  $\tau = 0.25$ , but were set at 0.30 and 0.20 respectively for CH1, CH2 and CH3, CH4 in relation with the same filling ratio (0.60 and 0.40) found for the phosphorus atoms. This change, which actually did not modify significantly the re-

TABLE IV  
REFINED TEMPERATURE FACTOR EXPRESSIONS ( $\beta$ 's)

Atom	$\beta_{11}$	$\beta_{22}$	$\beta_{33}$	$\beta_{12}$	$\beta_{13}$	$\beta_{23}$
Ta1	0.00208(2)	0.00497(9)	0.00086(1)	0.0005(2)	0.00206(3)	0.0015(1)
Ta1'	<i>a</i>			-0.0008(2)	0.00208(4)	-0.0014(1)
Ta2	0.00153(2)	0.0051(1)	0.00085(1)	-0.0015(2)	0.00148(3)	-0.0007(1)
Ta2'				0.0015(2)	0.00148(3)	0.0007(1)
S1	0.0044(1)	0.0057(7)	0.00144(5)	-0.002 (1)	0.0042 (2)	-0.0010(6)
S1'				-0.002 (1)	0.0042 (2)	-0.0007(7)
S2	0.0044(1)	0.0061(7)	0.00130(5)	-0.001 (1)	0.0043 (2)	-0.0005(6)
S2'				-0.003 (1)	0.0037 (2)	-0.0023(7)
S3	0.0029(1)	0.0084(8)	0.00189(6)	-0.007 (1)	0.0037 (2)	-0.0070(7)
S3'				0.004 (1)	0.0037 (2)	0.0042(7)
S4	0.0039(1)	0.0078(8)	0.00195(6)	-0.001 (1)	0.0044 (2)	-0.0012(7)
S4'				-0.003 (1)	0.0048 (2)	-0.0022(7)
S5	0.0026(1)	0.0066(7)	0.00128(6)	0.001 (1)	0.0025 (2)	0.0030(7)
S5'				0.001 (1)	0.0024 (2)	-0.0009(7)
S6	0.0033(1)	0.0076(7)	0.00126(5)	0.003 (1)	0.0033 (2)	0.0006(7)
S6'				-0.004 (1)	0.0033 (2)	-0.0033(7)
S7	0.0023(1)	0.0073(7)	0.00145(7)	-0.001 (1)	0.0015 (2)	-0.0022(8)
S7'				-0.002 (1)	0.0020 (2)	-0.0001(7)
S8	0.0015(1)	0.0056(7)	0.00117(7)	0.003 (1)	0.0015 (2)	0.0022(7)
S8'				-0.0015(9)	0.0013 (2)	-0.0004(7)
S9	0.0031(1)	0.0080(8)	0.00109(6)	0.002 (1)	0.0022 (2)	0.0000(7)
S9'				-0.004 (1)	0.0021 (2)	0.0003(7)
S10	0.0030(1)	0.0088(9)	0.00089(6)	-0.002 (1)	0.0022 (2)	0.0014(7)
S10'				0.001 (1)	0.0020 (2)	0.0003(7)
S11	0.0023(1)	0.0070(7)	0.00141(6)	-0.005 (1)	0.0020 (2)	-0.0051(8)
S11'				-0.000 (1)	0.0026 (2)	0.0017(7)
S12	0.0030(1)	0.0063(7)	0.00139(6)	0.0045(9)	0.0032 (2)	0.0021(7)
S12'				-0.002 (1)	0.0028 (2)	-0.0014(7)
Se-S1						
Se-S1'						
Se-S2						
Se-S2'						
Se-S7						
Se-S7'						
Se-S8						
Se-S8'						

Note. The form of the anisotropic thermal parameter is:  $\exp[-(\beta_{11}h^2 + \beta_{22}k^2 + \beta_{33}l^2 + \beta_{12}hk + \beta_{13}hl + \beta_{23}kl)]$ .

<sup>a</sup>  $\beta_{ij}$ 's for primed atoms were constrained to the values of unprimed atoms.

<sup>b</sup>  $\beta_{ij}$ 's and  $\beta_{ij}$  for the Se-S atoms were constrained to the values of the sulfur atoms they substitute.

finement results, was introduced because it was felt to correspond to better internal structure coherence.

Last calculation cycles led to  $R = 0.050$ , the Fourier difference map showing only some electronic distribution around the tantalum atoms ( $\sim 3.8(5) e/\text{\AA}^3$ ) attributable to incompletely corrected absorption. The final positional and thermal atomic parameters of TaPS<sub>6</sub>Se are collected in Tables IV and V.

## 5. Structural Results and Discussion

Before any other considerations, it is important to compare the crystal composition

obtained from the structure determination and that gathered from the microprobe analysis. Following the above structure determination steps, we have, from the BTS composition Ta<sup>VPV</sup>(S<sub>2</sub>)<sup>-II</sup>S<sub>4</sub><sup>-II</sup>, substituted the S<sub>2</sub><sup>-II</sup> pairs by selenium and obtained Ta<sup>V</sup>PV(S<sub>1.9</sub>Se<sub>0.1</sub>)<sup>-II</sup>S<sub>4</sub><sup>-II</sup>. Introduction of sulfur-substituted selenium chains (Se<sub>8</sub>S<sub>2</sub>), i.e., Se S<sub>0.25</sub> per tantalum, led to the overall composition Ta<sup>V</sup>PV(S<sub>1.9</sub>Se<sub>0.1</sub>)<sup>-II</sup>S<sub>4</sub><sup>-II</sup> (Se<sup>0</sup>S<sub>0.25</sub><sup>0</sup>) that is TaPS<sub>6.15</sub>Se<sub>1.1</sub>. If one compares the theoretical weight fraction concentration of this composition and of that of the stoichiometric formula PTaPS<sub>6</sub>Se, (Table I), one sees that little change is introduced in the P, S, and Ta concentrations, only that of sele-

TABLE V  
POSITIONAL PARAMETERS AND THEIR ESTIMATED STANDARD DEVIATIONS

Atom	$\tau$	X	Y	Z	B ( $\text{\AA}^2$ )	Atom	$\tau$	X	Y	Z	B ( $\text{\AA}^2$ )
Ta1	1	0.0044(16)	0.442	0.82724(4)	0.88(1)	P3	0.6	0.8047 (7)	0.369 (2)	0.4871 (5)	1.0(1)*
Ta1'	1	0.00426(6)	0.5586(2)	0.67702(4)	0.9	P3'	0.4	0.191 (1)	0.659 (3)	0.0114 (8)	1.0
Ta2	1	0.35011(6)	0.0578(2)	0.67304(5)	0.90(1)	P4	0.6	0.8043 (7)	0.637 (2)	0.8182 (5)	0.9(1)*
Ta2'	1	0.65024(6)	0.9413(2)	0.82308(5)	0.9	P4'	0.4	0.193 (1)	0.344 (3)	0.6811 (8)	0.9
S1	0.95	0.1016 (4)	0.277 (1)	0.7820 (3)	1.36(8)	S-CH1	0.3	0.393	0.515	0.949	3.4(4)*
S1'	0.95	0.9094 (4)	0.741 (1)	0.7216 (3)	1.4	Se1-CH1	0.3	0.478	0.696	0.039	6.0(2)*
S2	0.95	0.1016 (4)	0.742 (1)	0.8196 (3)	1.27(7)	Se2-CH1	0.3	0.424	0.889	0.932	5.7(2)*
S2'	0.95	0.9110 (5)	0.277 (1)	0.6892 (3)	1.5	Se3-CH1	0.3	0.429	0.112	0.995	5.8(2)*
S3	1	0.7824 (5)	0.419 (1)	0.7495 (3)	1.53(9)	Se4-CH1	0.3	0.474	0.322	0.937	5.9(2)*
S3'	1	0.2211 (4)	0.598 (1)	0.7474 (3)	1.5	S-CH2	0.3	0.503	0.013	0.554	3.3(4)*
S4	1	0.7241 (5)	0.911 (1)	0.7508 (3)	1.60(9)	Se1-CH2	0.3	0.601	0.196	0.562	5.7
S4'	1	0.2816 (4)	0.091 (1)	0.7496 (3)	1.5	Se2-CH2	0.3	0.559	0.390	0.491	6.0
S5	1	0.0012 (5)	0.112 (1)	0.8704 (3)	1.29(8)	Se3-CH2	0.3	0.563	0.610	0.568	5.9
S5'	1	0.0011 (5)	0.890 (1)	0.6301 (3)	1.3	Se4-CH2	0.3	0.601	0.819	0.537	5.8
S6	1	-0.0001 (5)	0.642 (1)	0.9167 (3)	1.31(8)	S-CH3	0.2	0.504	0.015	0.950	3.3
S6'	1	0.9992 (5)	0.358 (1)	0.5831 (3)	1.3	Se1-CH3	0.2	0.399	0.181	0.961	5.8
S7	0.95	0.4627 (5)	0.764 (1)	0.7757 (3)	1.7(1)	Se2-CH3	0.2	0.440	0.392	0.933	5.9
S7'	0.95	0.5346 (5)	0.227 (1)	0.7170 (3)	1.5	Se3-CH3	0.2	0.439	0.618	0.005	6.0
S8	0.95	0.5337 (5)	0.241 (1)	0.8109 (3)	1.14(9)	Se4-CH3	0.2	0.400	0.823	0.938	5.7
S8'	0.95	0.4631 (4)	0.776 (1)	0.6804 (3)	1.2	S-CH4	0.2	0.606	0.498	0.550	3.4
S9	1	0.7783 (5)	0.415 (1)	0.0262 (3)	1.52(9)	Se1-CH4	0.2	0.522	0.695	0.562	5.9
S9'	1	0.2181 (5)	0.592 (1)	0.4676 (3)	1.6	Se2-CH4	0.2	0.573	0.890	0.506	5.8
S10	1	0.7152 (5)	0.919 (1)	0.9662 (3)	1.40(9)	Se3-CH4	0.2	0.572	0.116	0.567	5.7
S10'	1	0.2728 (5)	0.099 (1)	0.5247 (3)	1.5	Se4-CH4	0.2	0.525	0.330	0.461	6.0
S11	1	0.8343 (5)	0.144 (1)	0.9167 (4)	1.49(9)	Se-S1	0.05	1.102	1.277	0.782	1.4
S11'	1	0.1670 (4)	0.858 (1)	0.5830 (3)	1.3	Se-S1'	0.05	1.909	1.741	0.722	1.4
S12	1	0.7402 (4)	0.613 (1)	0.8693 (3)	1.25(8)	Se-S2	0.05	1.102	1.742	0.820	1.3
S12'	1	0.2599 (5)	0.392 (1)	0.6290 (3)	1.4	Se-S2'	0.05	1.911	1.277	0.689	1.5
P1	0.6	0.1693 (8)	0.139 (2)	0.9883 (5)	1.2(1)*	Se-S7	0.05	1.463	1.764	0.776	1.7
P1'	0.4	0.830 (1)	0.850 (3)	0.5135 (8)	1.2	Se-S7'	0.05	1.535	1.227	0.717	1.5
P2	0.4	0.1682 (7)	0.864 (2)	0.6795 (5)	1.0(1)*	Se-S8	0.05	1.534	1.241	0.711	1.1
P2'	0.4	0.830 (1)	0.155 (3)	0.8157 (8)	1.0	Se-S8'	0.05	1.463	1.776	0.680	1.2

Note. Starred atoms were refined isotropically.  $\tau$ , occupancy ratio. Anisotropically refined atoms are given in the form of the isotropic equivalent thermal parameter defined as:  $B_{\text{eq}} = \frac{1}{3} \sum_i \beta_i a_i^2$ .



an overall structural viewpoint it must be pointed out that Ta<sub>4</sub>P<sub>4</sub>S<sub>29</sub> BTS is composed of two interlocking systems (see above), whereas the partial occupancy by phosphorus of all available tetrahedral sites seems to remove that special characteristic in TaPS<sub>6</sub>Se BTS. In fact, one set of phosphorus positions (that is occupied at 60%) corresponds to a right-hand rotation of the BTS tunnels and the other (40%) to a left-hand rotation and it is possible to imagine the crystal as made, at the microscopic level, by both types of arrangement. The compound would still then have an interlocked structure and, in addition, each type of tunnel would accompany the chalcogen helix having the same rotation direction. This would fit with the observation made on Ta<sub>4</sub>P<sub>4</sub>S<sub>29</sub> where the (S<sub>10</sub>) helix rotates like the BTS itself. This explains and justifies the choice of the occupancy ratio taken for the four helices in TaPS<sub>6</sub>Se during the last step of the refinement calculation. The assumption of coupled rotation is supported by the Ta<sub>2</sub>P<sub>2</sub>S<sub>11</sub> structure (19) where a large tunnel was found empty in relation to non-rotating coordination groups.

From a symmetry point of view, the monoclinic distortion may be attributed, to some extent, to the selenium substitution in the TaPS<sub>6</sub>Se BTS. Curiously, this substitution, although weak, seems to take place mostly on the (S<sub>2</sub>)<sup>-II</sup> pairs of the structure, with the consequence of elongating the calculated atomic distance to  $d_{S-S} = 2.116 \text{ \AA}$  (mean value) from  $d_{S-S} = 2.044 \text{ \AA}$ , for example, in Ta<sub>4</sub>P<sub>4</sub>S<sub>29</sub>. Correlatively, one finds a mean Ta-Ta length of  $d_{Ta-Ta} = 3.426 \text{ \AA}$  to be compared to  $3.384 \text{ \AA}$  in the selenium-free phase. To justify further the only substitution of the dianionic sulfur groups by selenium, one can compare the Ta-S distances between the substituted and unsubstituted sulfur atoms. To do that, we compare separately the mean Ta-S bond lengths between the cation and respectively the S<sub>2</sub><sup>-II</sup> and S<sup>-II</sup> anions.

For Ta<sub>4</sub>P<sub>4</sub>S<sub>29</sub> one finds

$$d_{Ta-S(\text{pairs})} = 2.560(6) \text{ \AA} \\ \text{and } d_{Ta-S(\text{single})} = 2.517(6) \text{ \AA}$$

and for TaPS<sub>6</sub>Se,

$$d_{Ta-S(\text{pairs})} = 2.600(6) \text{ \AA} \\ \text{and } d_{Ta-S(\text{single})} = 2.524(6) \text{ \AA}.$$

It appears clearly that the Ta-S distances of unsubstituted anions remain the same within error.

A lowering of the symmetry upon selenium substitution in Ta<sub>4</sub>P<sub>4</sub>S<sub>29</sub> from a tetragonal cell to a monoclinic one is expected to lead to some kind of distortion among the constituting groups of TaPS<sub>6</sub>Se, [Ta<sub>2</sub>S<sub>12</sub>], and [PS<sub>4</sub>] units. This is particularly noticeable on the eight different tetrahedra of the unit cell, and one can observe (Table VI) a rather wide dispersion of the P-S bond lengths from 1.99(1) to 2.18(1) Å, much more important than in Ta<sub>4</sub>P<sub>4</sub>S<sub>29</sub> (2.016(5) to 2.069(6) Å). Moreover, the mean P-S distance is larger (mean  $d_{P-S} = 2.09 \text{ \AA}$ ) in PTaS<sub>6</sub>Se than in Ta<sub>4</sub>P<sub>4</sub>S<sub>29</sub> (mean  $d_{P-S} = 2.04 \text{ \AA}$ ). This indicates that the [Ta<sub>2</sub>S<sub>12</sub>] units have become more separated and may be attributed, in agreement with the increase in cell parameters, to the selenium insertion within the tunnel.

Let us examine now the characteristics of the selenium and sulfur atoms located in the tunnels. These chalcogens form infinite helicoidal chains (Figs. 6 and 7) developing in the *b* direction from a group of 10 atoms (8 Se and 2 S) according to the sequence . . . -S-Se<sub>4</sub>-(S-Se<sub>4</sub>-S-Se<sub>4</sub>)-(S-Se<sub>4</sub> . . . . Although having a 2*b* periodicity, the (S-Se<sub>4</sub>-S-Se<sub>4</sub>) groups do not create a superstructure as the (S<sub>10</sub>) helix in Ta<sub>4</sub>P<sub>4</sub>S<sub>29</sub>. In effect half of the helices is the image of the other half through a 180° rotation, and since two helices are linked by a two-fold axis going through the tunnel center, the *b* periodicity is reestablished.

Each tunnel contains one right- and one left-hand helicoidal chain, and this is to be related to the phosphorus distribution. It is believed that the crystal may contain left- and right-hand microdomains with the corresponding helices. In effect, starting from  $\text{Ta}_4\text{P}_4\text{S}_{29}$ , one finds only van der Waals distances between BTS and chains, and one may assume that if the ( $\text{S}_{10}$ ) chain develops in an orderly manner, it is due to a kind of steric pressure since such chains can only be obtained, for the element, under high pressure. The rotating tunnel frame of the BTS then must impose its own orientation, hence the coupled rotation. Notwithstanding, the same phenomenon must take place in  $\text{TaPS}_6\text{Se}$  with helices accompanying the BTS.

The mean Se–Se distance ( $d_{\text{Se-Se}} = 2.31 \text{ \AA}$ ) and the mean Se–Se–Se angle ( $104^\circ$ ) are in good agreement with generally reported values, in particular for elemental selenium in its polymeric form ( $d_{\text{Se-Se}} = 2.32 \text{ \AA}$  and  $\text{Se–Se–Se} = 105^\circ$ ). In the same way, the mean sulfur–selenium bond length of  $d_{\text{S-Se}} = 2.22 \text{ \AA}$  falls between  $2.18 \text{ \AA}$  as observed in cyclotriselenium pentasulfur (20) and  $2.26 \text{ \AA}$  calculated in the selenotrichion (21). One observes that the expected Se–Se–Se bond angle of  $104^\circ$  is much larger than the S–Se–Se and Se–S–Se angles of  $97^\circ$ . For these angles, an important squeeze is operated by the structure, in order to have the helices commensurate with the crystal  $b$  direction. In spite of the decrease of these angles, the chalcogens located at their tips still show acceptable distances between  $3.33$  and  $3.47 \text{ \AA}$ .

It is remarkable that the angle shrinking takes place only for those mixed chalcogen groups as though only the sulfur substitution allowed it. This may be the origin of the sulfur substitution observed, the purely selenated chains being incompatible with the size and length in the tunnels. Then both ( $\text{TaPS}_6$ ) and ( $\text{Se}$ ) systems correlatively modify themselves to finally allow an energetically favorable solution without dis-

commensuration, with the result that the BTS widens through a sulfur–selenium substitution, the chain lowering its development parameter through selenium–sulfur substitution. This sheds a light on the property of adaptability of these Ta–P–X anisotropic tridimensional systems.

All the above results have however been obtained through special procedures, and only separated and constrained variable refinement could be done. This may, in part, explain the relatively high isotropic thermal factors of the chains atoms (Table V), although this was observed before, for instance in  $\text{Ta}_4\text{P}_4\text{S}_{29}$ , in the sulfur chain. The importance of these thermal factors may also be related, to some degree, to miscommensuration and/or to some small statistical substitution on the chain selenium sites. It was felt thus useful to undergo some infrared and Raman spectroscopy studies to confirm the X-ray diffraction interpretation.

## 6. Vibrational Spectroscopic Investigations

At first glance, Raman and IR spectra of  $\text{TaPS}_6\text{Se}$  show remarkable similarity in the whole frequency range with those of  $\text{TaPS}_6$  and  $\text{Ta}_4\text{P}_4\text{S}_{29}$  both in the general pattern and in the frequencies of the bands (22). This suggests that the observed spectra originate from the same species namely the internal modes of the  $[\text{PS}_4]$  groups and the  $[\text{Ta}_2(\text{S}_2)_2]$  units. It must be underlined that for vibrational study, an approach to the band assignment can be successfully done from these two groups considered separately (22),  $[\text{PS}_4]$  being the classical tetrahedral group and  $[\text{Ta}_2(\text{S}_2)_2]$  the cluster made of two Ta atoms and a  $(\text{S}_2)^{-11}$  rectangle. Nevertheless, it must be pointed out that the signals between  $460$  and  $466 \text{ cm}^{-1}$  assigned to  $\nu_{\text{S-S}}$  within the sulfur chain in  $\text{Ta}_4\text{P}_4\text{S}_{29}$  are now missing. The assignment of the bands related to the  $[\text{Ta}_2(\text{S}_2)_2]$  cages is discussed in a forthcoming paper (22).

In TaPS<sub>6</sub>Se spectra, the low multiplicity of frequencies gives evidence of weak vibrational couplings within the unit cell as expected theoretically by  $Z = 8$ . Strong interactions must be localized within the tetrahedral [PS<sub>4</sub>] groups in spite of their closeness to Ta atoms. As a matter of fact, characteristic frequencies with relatively well-known intensities appear clearly in the spectra. [PS<sub>4</sub>] groups are in general position but simple correlation with factor group  $C_2$  should cause splitting of each mode into two components A and B both IR and Raman active.

Crystal field and/or distortion from a perfect tetrahedron appear sufficient to remove partially the degeneracy of the  $F_2$  mode and to affect selection rules. The highest frequencies from 560 to 598 cm<sup>-1</sup> are assigned to the antisymmetric stretching  $\nu_a(F_2)$  mode with three intense IR absorption bands in particular.  $\delta(F_2)$  mode gives rise to an intense IR doublet at 319–312 cm<sup>-1</sup> and several weak Raman signals between 296 and 324 cm<sup>-1</sup> whereas the  $\nu_s(A_1)$  mode becomes IR active (single weak signal at 424 cm<sup>-1</sup>). A single band near 277 cm<sup>-1</sup> is assigned to  $\delta(E)$  mode.

Care must be taken in discussing scattering and values of  $\nu_a$  and  $\nu_s$ P–S frequencies. They seem to show, in spite of a slight shift toward low frequencies, neither a larger dispersion of P–S bond lengths in TaPS<sub>6</sub>Se than in Ta<sub>4</sub>P<sub>4</sub>S<sub>29</sub> nor the lengthening of the P–S interatomic mean distance from 2.044 Å (for Ta<sub>4</sub>P<sub>4</sub>S<sub>29</sub>) to 2.088 Å (for TaPS<sub>6</sub>Se). Moreover,  $\nu$ P–S values of TaPS<sub>6</sub>Se are approximately the same as for TaPS<sub>6</sub> which displays significantly shorter P–S bonds.

As far as the Ta<sub>2</sub>(S<sub>2</sub>)<sub>2</sub> cluster modes are concerned,  $\nu S_2^{2-}$  frequencies (two Raman signals at 544 and 523 cm<sup>-1</sup> and an IR counterpart at 540 cm<sup>-1</sup>) yield a S–S distance of 2.055 and 2.075 Å according to Steudel's empirical equation (23) (already well obeyed by TaPS<sub>6</sub> and Ta<sub>4</sub>P<sub>4</sub>S<sub>29</sub>). If compared to the corresponding S–S bond lengths for these two last sulfides (same

mean values of 2.04 Å), these values prove to be significantly longer. This difference is quite in line with the statistical substitution by selenium within the S<sub>2</sub> pairs as found by the structural study.

Stretching modes of Se–Se pairs are expected to occur, with high Raman efficiency compared to sulfur pairs (24), at about 300 cm<sup>-1</sup> according to available data for ZrSe<sub>3</sub>, HfSe<sub>3</sub>, ZrS<sub>3-x</sub>Se<sub>x</sub> (24, 25). A careful comparison of the spectra of Ta<sub>4</sub>P<sub>4</sub>S<sub>29</sub> and TaPS<sub>6</sub>Se between 180 and 450 cm<sup>-1</sup> deserve some comments. First, we do observe an intense IR absorption at about 290 cm<sup>-1</sup> with a weak Raman counterpart. Unfortunately, deformation modes of [PS<sub>4</sub>] group give rise to strong features in this frequency field and this peak might stem from a further splitting of  $\delta(F_2)$  or ( $E$ ) modes. Moreover, the strong doublet dominating the Raman spectrum of TaPS<sub>6</sub>Se at 351–343 cm<sup>-1</sup> is straightforwardly assigned to the totally symmetric  $A_g\nu Ta(S_2)_2$  mode with contribution of the  $B_{2g}\nu TaS_2$  mode. The frequencies, slightly lower than those concerning Ta<sub>4</sub>P<sub>4</sub>S<sub>29</sub>, agree quite well with Ta–S bonds longer in the selenium compound. However, no structure attributable to a possible  $A_g\nu Ta(Se_2)_2$  mode or  $\nu TaSe_2$  mode was detected.

The remaining deformation modes of Ta (S<sub>2</sub>)<sub>2</sub> units are found below 270 cm<sup>-1</sup> as single bands at frequencies very close to that observed for Ta<sub>4</sub>P<sub>4</sub>S<sub>29</sub>.

An estimation of the (Se–S)<sup>2-</sup> mode frequency (within pairs) suggested by Zwick *et al.* (25) may be obtained with a rather good approximation by

$$\omega^2(\text{Se-S}) = \frac{1}{2}[\omega^2(\text{S-S}) + \omega^2(\text{Se-Se})].$$

With  $\sigma(S_2)^{-II} = 540$  cm<sup>-1</sup> and  $\nu(Se_2)^{-II} = 300$  cm<sup>-1</sup>, this relation gives a wave number equal to 437 cm<sup>-1</sup> for  $\nu(\text{Se-S})$ . An additional peak, located in the high-frequency part in the IR spectrum at 446 cm<sup>-1</sup>, might originate from such a mode. But, we do not observe the Raman counterpart, making this assignment somewhat speculative.

Next, a new structure appears clearly at  $368\text{ cm}^{-1}$  in the IR spectrum and at  $375\text{ cm}^{-1}$  as a weak Raman signal. These positions are consistent with available data on  $\nu\text{Se-S}$  for  $\text{S}_n\text{Se}_{8-n}$  and  $\text{Se}_n\text{Se}_{6-n}$  molecules, the values of which are reported in the region  $345\text{--}382\text{ cm}^{-1}$  (26, 27). This identification, along with the missing signals of  $\nu\text{S-S}$  ( $460\text{--}466\text{ cm}^{-1}$  for  $\text{Ta}_4\text{P}_4\text{S}_{29}$ ) and  $\delta_{\text{S}}^{\text{S}}\text{S}$  (strong Raman line at  $161\text{ cm}^{-1}$  for this same compound) is quite consistent with the occupancy of the channels by a mixed chalcogen chain, the sulfur atoms being only involved in Se-S bonds.

Further spectroscopic characterization of this chain has been done to support the structural conclusions and the above assignment. Back-scattering experiments using Raman micromole were performed with the propagation direction of the  $p$ -polarized incident light perpendicular to the  $b$  axis growth of a single crystal. Change of orientation of the crystal shows, in the low frequency field, the high Raman efficiency of lines at  $235$  and  $262\text{ cm}^{-1}$ . Although these experiments do not allow us to separate the contributions of the derived polarizability tensor and the  $A$  and  $B$  modes in the  $C_2^1$  group, they reveal a striking intensity correlation between the line at  $262\text{ cm}^{-1}$  and the Raman signal at  $343\text{ cm}^{-1}$  associated to the fully symmetric  $A_g\nu\text{Ta}(\text{S}_2)_2$  mode.

It is thus possible to assign the peak at  $262\text{ cm}^{-1}$  to the symmetric  $\nu\text{Se-Se}$  mode within the chain and the peak at  $235\text{ cm}^{-1}$  to the antisymmetric mode. These assignments are well supported by the location of the  $\nu\text{Se-Se}$  mode in metallocycloselenanes  $C_pM\text{Se}_5$  ( $C_p = n\text{C}_5\text{H}_5$ ,  $M = \text{Ti, Zr, Hf}$ ) at  $261\text{--}266$  and  $245\text{--}248\text{ cm}^{-1}$  (symmetric and antisymmetric modes, respectively) and in  $\text{Se}_2\text{S}_5$  at  $271\text{ cm}^{-1}$  (28). A rather good agreement is also found with the  $\nu\text{Se-Se}$  frequency calculated at  $259\text{ cm}^{-1}$  using the Se-Se mean bond length of  $2.305\text{ \AA}$  (see structural result) and the empirical relation proposed by Butler *et al.* (28).

$$\nu\text{Se-Se} = 901.7 - 279.0[r(\text{Se-Se})]$$

Otherwise, in these single-crystal spectra, the intensities of the  $544\text{-cm}^{-1}$  line  $\nu(\text{S}_2)^{-\text{II}}$  and of the  $290\text{-cm}^{-1}$  line do not display the same behavior. This finding confirms—as proposed above—that the last signal cannot originate from  $\nu(\text{Se}_2)^{-\text{II}}$  within pairs and suggests random substitution into the  $(\text{S}_2)^{-\text{II}}$  pairs.

With this  $\nu\text{Se-Se}$  frequency within chains ( $262\text{ cm}^{-1}$  as a mean value) and  $\nu\text{S-S}$  frequency ( $\sim 463\text{ cm}^{-1}$ ), a calculated value of  $\nu\text{Se-S} = 370\text{ cm}^{-1}$  is obtained using the above relation between the three frequencies. This value confirms previous assignment of the peaks at  $368\text{ cm}^{-1}$  (IR) and  $375\text{ cm}^{-1}$  (Raman) to such a mode.

From the above structural and spectroscopic data, the particular features of  $\text{TaPS}_6\text{Se}$  have been determined and the occurrence of inserted and partially substituted selenium chains demonstrated. The occurrence of these neutral chalcogen chains within the tunnel of  $\text{TaPS}_6\text{Se}$  can be supported by magnetic measurements. From interatomic distance considerations, and ignoring the slight selenium substitution in the  $(\text{S}_2)^{-\text{II}}$  pairs of the BTS, one obtains the developed formula  $\text{Ta}^{\text{V}}\text{P}^{\text{V}}(\text{S}_2)^{-\text{II}}\text{S}_4^{-\text{II}}\text{Se}^0\text{S}_{1/4}^0$ . With  $d^0$  tantalum, the phase has to be diamagnetic and this is found with  $\chi_{295\text{ K}} = -100 \times 10^{-6}$  u.e.m. with a consistent room temperature high resistivity greater than  $10^9\ \Omega\text{ cm}$ .  $\text{TaPS}_6\text{Se}$  is thus closely related to  $\text{Ta}_4\text{P}_4\text{S}_{29}$  and presents the same charge balance. Although selenium-substituted rings have already been synthesized, this is the first time that selenium-sulfur chains are found.

## 7. Conclusion

Substitution by selenium of the sulfur chain inserted in  $\text{Ta}_4\text{P}_4\text{S}_{29}$  was successfully achieved. The new phase obtained ( $\approx \text{TaPS}_{6.15}\text{Se}_{1.1}$ ) presents a monoclinic symmetry corresponding to a distortion of the original

tetragonal cell of the nonsubstituted sulfide to which it is closely related. TaPS<sub>6</sub>Se BTS undergoes a small sulfur substitution on some specific sulfur sites constituted by the sulfur anionic pairs, indicating a preferential action of selenium on these groups. Vibrational (IR and Raman) studies seem to indicate a random selenium distribution in these pairs resulting in the occurrence of (S–Se) groups rather than (Se<sub>2</sub>) pairs. This substitution allows an increase of the tunnel size that, along with some substitution by sulfur in the selenium chains, the composition of which becomes (Se<sub>4</sub>S)<sub>x</sub>, explains the actual commensurate insertion of these polymeric groups in the compound. The spectroscopic studies also indicate, within the chalcogen chain, the only presence of Se–S and Se–Se bonds in agreement with the interpretation of the X-ray diffraction analysis which led to the conclusion of the occurrence of four different kinds of (Se<sub>8</sub>S<sub>2</sub>)<sub>x</sub> chains.

These chains are found randomly distributed within the BTS's tunnels. Right- and left-hand helices can be recognized and assumed to fill separately the tunnels and to rotate in the same way as the BTS coordination polyhedra, thus preserving the characteristics of Ta<sub>4</sub>P<sub>4</sub>S<sub>29</sub> features, in particular the interlocking of the structure. From these results and in agreement with the characteristics found for Ta<sub>2</sub>P<sub>2</sub>S<sub>11</sub> (19), it appears that the BTS rotating tunnel imposes the same rotation on the inserted chalcogen chain which is locked through a sort of steric pressure.

### Acknowledgment

The authors thank Dr. A. Meerschaut for decisive discussions in solving the present structure.

### References

1. S. FIECHTER, W. F. KUHS, AND R. NITSCHKE, *Acta Crystallogr. Sect. B* **36**, 2217 (1980).
2. M. EVAÏN, M. QUEIGNEC, R. BREC, AND J. ROUXEL, *J. Solid State Chem.* **56**, 148 (1985).
3. R. W. G. WYCKOFF, "Crystal Structure," Vol. 1, pp. 36–37, Interscience, New York (1975).
4. M. EVAÏN, M.-H. WHANGBO, AND R. BREC, to be published.
5. R. YVON, W. JEITSCHKO, AND E. PARTHE, *J. Appl. Crystallogr.* **10**, 73 (1977).
6. B. FRENZ, "Enraf–Nonius, Structure Determination Package," Delft Univ. Press, Delft (1982).
7. G. OUVVARD, R. BREC, AND J. ROUXEL, *Mater. Res. Bull.* **20**, 1181 (1985).
8. R. BREC, G. OUVVARD, AND J. ROUXEL, *Mater. Res. Bull.* **20**, 1257 (1985).
9. G. OUVVARD, R. FREOUR, R. BREC, AND J. ROUXEL, *Mater. Res. Bull.* **20**, 1053 (1985).
10. G. OUVVARD, R. BREC, AND J. ROUXEL, *Ann. Chim. (Paris)* **7**, 53 (1982).
11. R. BREC, G. OUVVARD, R. FREOUR, AND J. ROUXEL, *Mater. Res. Bull.* **18**, 689 (1983).
12. R. BREC, G. OUVVARD, M. EVAÏN, P. GRENOUILLEAU, AND J. ROUXEL, *J. Solid State Chem.* **47**, 174 (1983).
13. M. EVAÏN, R. BREC, G. OUVVARD, AND J. ROUXEL, *J. Solid State Chem.* **56**, 12 (1985).
14. R. BREC, M. EVAÏN, P. GRENOUILLEAU, AND J. ROUXEL, *Rev. Chim. Miner.* **20**, 283 (1983).
15. P. GRENOUILLEAU, R. BREC, M. EVAÏN, AND J. ROUXEL, *Rev. Chim. Miner.* **20**, 628 (1983).
16. R. BREC, P. GRENOUILLEAU, M. EVAÏN, AND J. ROUXEL, *Rev. Chim. Miner.* **20**, 295 (1983).
17. M. EVAÏN, R. BREC, G. OUVVARD, AND J. ROUXEL, *Mater. Res. Bull.* **18**, 41 (1984).
18. P. TOFFOLI, P. KHODADAD, AND N. RODIER, *Acta Crystallogr. Sect. B* **33**, 285 (1977).
19. M. EVAÏN, S. LEE, M. QUEIGNEC, AND R. BREC, *J. Solid State Chem.* **71**, 139 (1987).
20. R. LAITINEN, N. RAUTENBERG, J. STEIDEL, AND R. STEUDEL, *Z. Anorg. Allg. Chem.* **486**, 116 (1982).
21. A. F. WELLS, "Structural Inorganic Chemistry," 5th ed., p. 733, Oxford Univ. Press, London/New York (1984).
22. M. QUEIGNEC, J. SOURISSEAU, M. EVAÏN, AND R. BREC, to be published.
23. R. STEUDEL, *Angew. Chem. Int. Ed. Engl.* **14**, 655 (1975).
24. A. ZWICK, G. LANDA, R. CARLES, M. A. RENUCCI, AND A. KJESHUS, *Solid State Commun.* **45**, 889 (1983).
25. A. ZWICK, G. LANDA, M. A. RENUCCI, R. CARLES, AND A. KJESHUS, *Phys. Rev. B* **26**, 5694 (1982).
26. R. LAITINEN, R. STEUDEL, AND E. M. STRAUSS, *J. Chem. Soc. Dalton Trans.*, **9**, 1869 (1985).
27. R. LAITINEN AND R. STEUDEL, *J. Mol. Struct.* **68**, 19 (1980).
28. I. S. BUTLER, P. D. HARVEY, J. M. MCCALL, AND A. SHAVER, *J. Raman Spectrosc.* **17**, 221 (1986).